Title
Recurrent somatic mutations in ACVR1 in pediatric midline high-grade astrocytoma.

Journal
Nature Genetics, 46(5)

Authors
Fontebasso, Adam
Papillon-Cavanagh, Simon
Schwartzentruber, Jeremy
et al.

Publication Date
2014-05-01

DOI
10.1038/ng.2950

Peer reviewed

Published in final edited form as:
Nat Genet. 2014 May ; 46(5): 462–466. doi:10.1038/ng.2950.

Recurrent somatic mutations in *ACVR1* in pediatric midline high-grade astrocytoma

Adam M. Fontebasso[1,33], **Simon Papillon-Cavanagh**[2,33], **Jeremy Schwartzentruber**[3,33], **Hamid Nikbakht**[2], **Noha Gerges**[2], **Pierre-Olivier Fiset**[4], **Denise Bechet**[2], **Damien Faury**[2,5], **Nicolas De Jay**[2], **Lori Ramkissoon**[6], **Aoife Corcoran**[6], **David T W Jones**[7], **Dominik Sturm**[7], **Pascal Johann**[7], **Tadanori Tomita**[8], **Stewart Goldman**[9], **Mahmoud Nagib**[10], **Anne Bendel**[11], **Liliana Goumnerova**[12,13], **Daniel C. Bowers**[14], **Jeffrey R. Leonard**[15], **Joshua B. Rubin**[16], **Tord Alden**[8], **Samuel Browd**[17], **J. Russell Geyer**[18], **Sarah Leary**[18], **George Jallo**[19], **Kenneth Cohen**[20], **Nalin Gupta**[21], **Michael D. Prados**[21], **Anne-Sophie Carret**[22], **Benjamin Ellezam**[23], **Louis Crevier**[24], **Almos Klekner**[25], **Laszlo Bognar**[25], **Peter Hauser**[26], **Miklos Garami**[26], **John Myseros**[27], **Zhifeng Dong**[28], **Peter M. Siegel**[28], **Hayley Malkin**[29], **Azra Ligon**[13,30], **Steffen Albrecht**[4], **Stefan M. Pfister**[7], **Keith L. Ligon**[6,13,30,31,34], **Jacek Majewski**[2,34], **Nada Jabado**[1,2,5,34], and **Mark W Kieran**[13,27,32,34]

[1]Division of Experimental Medicine, Montreal Children's Hospital, McGill University and McGill University Health Centre, Montreal, Quebec, Canada

[2]Department of Human Genetics, McGill University, Montreal, Quebec, Canada

[3]Wellcome Trust Sanger Institute, Hinxton, UK

[4]Department of Pathology, Montreal Children's Hospital, McGill University Health Centre, Montreal, Quebec, Canada

[5]Department of Pediatrics, McGill University, Montreal, Quebec, Canada

[6]Department of Medical Oncology, Center for Molecular Oncologic Pathology, Dana-Farber Cancer Institute, Harvard University, Boston, Massachusetts, USA

[7]Division of Pediatric Neuro-oncology, German Cancer Research Center (DKFZ), Heidelberg, Germany

[8]Department of Neurological Surgery, Ann & Robert H. Lurie Children's Hospital of Chicago, Northwestern University, Chicago, Illinois, USA

[34]These authors jointly directed this work. Correspondence should be addressed to K.L.L. (keith_ligon@dfci.harvard.edu), J. Majewski (jacek.majewski@mcgill.ca), N.J. (nada.jabado@mcgill.ca) or M.W.K. (mark_kieran@dfci.harvard.edu)..
[33]These authors contributed equally to this work

Accession codes
Whole-exome sequencing data and DNA methylation data can be accessed through the European Genome-phenome Archive (EGA) at the following accession number: EGAS00001000720.

Author contributions
AMF, N. Gerges, POF, D. Bechet, DF, LR, AC, AL, SA, ZD performed experiments. AMF, SPC, JS, HN, NDJ, AL, SA, ZD, PMS analyzed the data and produced figures and tables. DTWJ, DS, PJ, TT, SG, MN, AB, LG, D. Bowers, JRL, JR, TA, SB, RG, GJ, KC, N. Gupta, MDP, ASC, BE, LC, AK, LB, PH, MG, J. Myseros, HM, SA, SMP provided tissue samples. KLL, J. Majewski, NJ, MWK provided project leadership and designed the study. All authors contributed to the final manuscript.

Conflict of Interest
The authors declare that they have no competing financial interests.

[9]Department of Pediatrics-Hematology, Oncology, Ann & Robert H. Lurie Children's Hospital of Chicago, Northwestern University, Chicago, Illinois, USA

[10]Neurosurgical Associates, Ltd., Children's Hospital and Clinics of Minnesota, Minneapolis, Minnesota, USA

[11]Department of Pediatric Hematology-Oncology, Children's Hospitals and Clinics of Minnesota, Minneapolis, Minnesota, USA

[12]Department of Neurosurgery, Boston Children's Hospital, Boston Massachusetts, USA

[13]Harvard Medical School, Boston, Massachusetts, USA

[14]Department of Pediatrics, University of Texas Southwestern Medical Center, Dallas, Texas, USA

[15]Department of Neurological Surgery, Washington University School of Medicine in St. Louis, St. Louis, Missouri, USA

[16]Department of Pediatrics, Hematology-Oncology, Washington University School of Medicine in St. Louis, St. Louis, Missouri, USA

[17]Department of Neurosurgery, Seattle Children's Hospital, Seattle, Washington, USA

[18]Cancer and Blood Disorders Center, Seattle Children's Hospital, Seattle, Washington, USA

[19]Department of Neurological Surgery, Johns Hopkins Hospital, Baltimore, Maryland, USA

[20]Department of Pediatric Hematology-Oncology, The Sidney Kimmel Comprehensive Cancer Center at Johns Hopkins, Baltimore, Maryland, USA

[21]Department of Neurological Surgery, University of California, San Francisco, San Francisco, California, USA

[22]Department of Hematology-Oncology, Centre hospitalier universitaire (CHU) Sainte-Justine, Universite de Montreal, Montreal, Quebec, Canada

[23]Department of Pathology, Centre hospitalier universitaire (CHU) Sainte-Justine, Universite de Montreal, Montreal, Quebec, Canada

[24]Department of Neurosurgery, Centre hospitalier universitaire (CHU) Ste-Justine, Universite de Montreal, Montreal, Quebec, Canada

[25]Department of Neurosurgery, Medical and Health Science Center, University of Debrecen, Debrecen, Hungary

[26]2nd Department of Paediatrics, Semmelweis University, Budapest, Hungary

[27]Department of Neurosurgery, Children's National Medical Center, Washington, DC, USA

[28]Rosalind and Morris Goodman Cancer Research Centre, McGill University, Montreal, Quebec, Canada

[29]Department of Pediatric Oncology, Dana-Farber Cancer Institute, Boston, Massachusetts, USA

[30]Department of Pathology, Brigham and Women's Hospital, Boston, Massachusetts, USA

[31]Department of Pathology, Boston Children's Hospital, Boston, Massachusetts, USA

[32]Division of Pediatric Hematology/Oncology, Boston Children's Hospital, Boston, Massachusetts, USA

Abstract

Midline pediatric high-grade astrocytomas (pHGAs) are incurable with few treatment targets identified. Most tumors harbor K27M mutations on histone 3 variants. In 40 treatment-naïve midline pHGAs, 39 analyzed by whole-exome sequencing, we find additional somatic mutations specific to tumor location. Gain-of-function mutations in *ACVR1* occur in tumors of the pons in conjunction with H3.1 K27M, while *FGFR1* mutations/fusions occur in thalamic tumors associated with H3.3 K27M. Hyper-activation of the bone morphogenetic protein (BMP)/ACVR1 developmental pathway in pHGAs harbouring *ACVR1* mutations led to increased phospho-SMAD1/5/8 expression and up-regulation of BMP downstream early response genes in tumour cells. Global DNA methylation profiles were significantly associated with the K27M mutation regardless of the mutant H3 variant and irrespective of tumor location, supporting its role in driving the epigenetic phenotype. This significantly expands the potential treatment targets and further justifies pre-treatment biopsy in pHGA as a means to orient therapeutic efforts in this disease.

We and others recently identified recurrent mutations in *H3F3A*, encoding histone 3 variant 3 (H3.3), in 38% of pediatric supratentorial high-grade astrocytomas (HGAs), and mutations in H3.3 or H3.1 in ~80% of brainstem HGA (diffuse intrinsic pontine gliomas, DIPG)[1–3]. Mutations of the histone H3 tail altering glycine 34 to either arginine or valine (G34R, G34V), as well as mutations in genes affecting H3 post-translational modifications (PTM) at lysine 36 predominate in cortical tumors, while lysine 27 to methionine (K27M) mutations occur in midline tumors[1,2,4,5].

Herein, we focus on the genomic (mutational spectrum, copy number alterations) and epigenetic (DNA methylation) landscape of treatment-naïve midline (thalamus, cerebellum, spine and pons; non-cortical regions) pediatric HGA. These tumors are often surgically challenging or inoperable, and published studies have mainly used post-therapy material and provided limited genomic data other than structural alterations and mutational analysis of H3 variants and *TP53*[1,3,6,7]. We analyzed 40 midline HGAs, with whole-exome sequencing (WES) data for 39 tumors, including 25 DIPG patient biopsies (11 previously reported[2,8], Table S1 and Online Methods). The recurrent H3 mutation K27M was found in 37/40 (93%) cases and was distributed among three histone variants including *H3F3A* (32/40 samples), *HIST1H3B* (4/39) and *HIST1H3C* (1/39). *HIST1H3C* also encodes the canonical H3.1 (as *HIST1H3B*) and has not been previously reported to be mutated (Figure 1). All five H3.1 mutations occurred in the pons of younger patients (Figure S1). H3.3 K27M mutations occurred in multiple midline locations, including the brainstem (19/25), thalamus (7/9) and rare locations for HGA – the cerebellum, 4th ventricle and spinal cord (4/4). In contrast, only one H3.3 K27M mutant was identified in 42 pHGAs located in the cerebral hemispheres in a previously reported dataset[3,5] (Figure 1, Table S1)

The pattern of somatic mutations in specific genes or gene pathways revealed striking features (Figure 1, Figure S1). Recurrent somatic mutations in the activin A receptor, type I

(*ACVR1*) occurred in 5/39 midline HGAs, and overlapped with K27M mutants (5/5), mainly H3.1 K27M (4/5) rather than H3.3 K27M or wild-type H3 tumors (p=0.0003, Fisher's exact test, Figure S1). The mutated amino acid residues in *ACVR1* have previously been reported as germline mutations causing fibrodysplasia ossificans progressiva (FOP), an inherited musculoskeletal disease[9–14]. The substitutions p.R206H, p.G328E, and p.G356D result in ligand-independent activation of the kinase leading to increase of bone morphogenetic protein (BMP) signaling and increased phospho-SMAD1/5/8 production in tissues[10], while the novel mutations p.G328V or p.R258G mutations are predicted to exert gain-of-function effects similar to the previously described mutations p.R258S or p.G328E/W/R, based on physico-chemical properties of the mutant residues and predicted protein structure (Figure 4 and Table S2)[11,12]. ACVR1, also known as ALK2, is a type I receptor of the mammalian TGF-β signalling family with critical developmental roles in the mouse embryo[13] and in early left-right patterning[14]. Investigation of ALK2 pathway activation using phospho-SMAD1/5/8 immunohistochemical staining in DIPG samples showed positive staining only in tumors with mutant *ACVR1* (4/4), including in the novel G328V and R258G DIPG mutants (Figure 2). In addition, in the primary cell line DIPGIV, which carries H3.1 K27M and the novel ACVR1 mutation G328V, we demonstrate increased phospho-SMAD1/5/8 levels compared to normal human astrocytes and a significantly increased expression of BMP response-element containing genes *ID1-3* and of *SNAI1* compared to KNS42, an H3.3 G34V mutant *ACVR1* wild-type cell line (Figure 4). These genes are early response genes induced following active BMP2 signaling and SMAD1/5/8 downstream effectors[15,16].

We identified mutations in *FGFR1* in association with H3.3 K27M mutation in 4/39 cases: 3 thalamic HGAs also having *NF1* mutations (previously reported in[8]) and one DIPG (Figure 1). These *FGFR1* mutations occurred at hotspot residues in the tyrosine kinase domain of the FGFR1 receptor. They have been shown to lead to its constitutive activation in a subset of thalamic pilocytic astrocytoma, a grade I tumor which rarely progresses to higher-grade astrocytomas, and in NIH 3T3 cells[8]. Comparison with our dataset of non-midline cortical pHGAs indicated tumors carrying H3.1, *ACVR1* or *FGFR1* mutations to be exclusive to midline HGA (p=0.0040, Fisher's exact test, Figure 1, Figure S1b).

TP53 mutations occurred in 29/39 samples, largely in combination with H3.3 K27M (23/27) as reported previously[1,2] and to a much lesser extent with H3.1 K27M (1/5) (Figure 1, Figure S1b). One DIPG sample (mHGA1) had H3.3 K27M as well as a splicing mutation in *CHEK2*, a gene associated with Li-Fraumeni syndrome similar to *TP53* (Figure 1, Tables S1, S6). Three midline samples displayed no detectable mutation across *H3F3A/HIST1H3B*/*HIST1H3C*, even when sequenced at extremely high depth (average read depth across all tumors/genes >20,000X, Table S3). They carried alterations described in adult HGA in the form of combined *TP53* mutation, *PDGFRA* amplification, and *CDKN2A* loss (mHGA35), *PDGFRA* and *EGFR* amplifications and *NF1* loss (mHGA36), or the previously identified *FGFR1-TACC1* fusion[17,18] (mHGA37) (Figure 1, Tables S1, S3–S4).

Somatic *PDGFRA* mutations were identified in a small subset of midline pHGA (5/39, Table S1). Notably, *PDGFRA* amplification occurred in 3/12 treatment-naïve DIPGs (Figure S2, Table S1). Interestingly, a cerebellar HGA sample where multiple biopsies were taken from different anatomical loci showed *PDGFRA* amplification in only one tumor site, while

strikingly similar somatic mutation and DNA methylation profiles across all tumor sites were observed (Figure S3). This supports the view that *PDGFRA* amplifications precede therapy but can be further promoted by it as described in radiation-induced supra-tentorial HGA[19]. Other growth factor receptors and components described to have focal gains/losses in DIPG[6,7] or HGA (*MET*, *RB*, *PARP1*) showed low incidence in our dataset (Figure 1, Tables S1, S4–S6) while recurrent mutations in components of the PI3K pathway, predicted to activate AKT signaling, were present in 10/39 midline HGA. Regarding alterations affecting telomere length, *ATRX* mutations were identified in 9 midline tumors, exclusively in H3.3 K27M-*TP53* mutant samples and affected older children[1] while no *TERT*-promoter mutations, assessed using targeted sequencing, were identified in midline pHGAs (Table S1).

K-to-M substitutions in histone variants at residue K27 have recently been shown to inhibit SET-domain containing histone methyltransferases[20], possibly accounting for the specific DNA methylation pattern we observed in H3.3 K27M non-brainstem tumors[4]. When clustering our samples by global DNA methylation, all samples with a given H3 mutation (K27, G34 or absent) clustered together, but did not group based on tumor location within the brain, the particular H3 gene mutated, and additional partner mutations or structural alterations identified (Figure 3 and Figure S5–S6). The global epigenetic profile is thus strongly associated with the alteration in the histone 3 variant mark. Interestingly, *TP53* alteration was associated with increased broad copy number changes as we previously showed[2] (average of 32 events per sample) indicating a level of genomic instability. This number was significantly higher in H3.3 G34R/V mutant samples compared to other groups (Table S7), in keeping with global hypomethylation identified in these tumors[4].

The gain-of-function alterations in three growth factor receptors, *ACVR1*, *FGFR1* and *PDGFRA*, associate with H3 K27M variants in midline HGA. These mutations are not seen concurrently, and *ACVR1* and *FGFR1* mutations are mutually exclusive with *TP53* alterations and privilege specific locations within the midline of the brain. ACVR1 mutations do not seem to correlate with differential survival in patients with HGA, although no definite conclusions can be drawn based on our limited sample size (Figure S4). The lack of reported CNS tumor development in FOP patients or Acvr1/Alk2 mouse models suggests that aberrant activation of this pathway is not sufficient for tumorigenesis[10] and may act in concert with H3 K27M mutations and other alterations we identify in the PI3K pathway in these tumors to induce tumorigenesis (Figure 1). Interestingly, *ACVR1* is mainly expressed at E14 in the cortex of mouse embryos and at very low level in the brainstem, and aberrantly active ACVR1 leads to increased ventralization of zebrafish embryos[11,12,21]. Aberrant ACVR1 signaling in the brainstem, a midline structure for a gene involved in left-right patterning, may potentially specify a patterning defect in DIPG. FGFR signaling regulates neural progenitor maintenance and the development of the ventral midbrain[22]. Similar to ACVR1 mutations, the FGFR1 gain-of-function mutations we identify only lead to grade I astrocytomas if present on their own in a tumor[8], and are commonly found in association with *NF1* and H3.3 K27M mutations in midline HGA. Mutations in H3 variants in pediatric HGAs mirror *IDH*-mutations in their requirement for additional alterations to potentially induce HGA. G34R/V mutations are found in *H3F3A* and not in other histone genes to date,

and invariably associate with *TP53* and *ATRX* mutations in the cortex. In midline pHGA, K27M mutations arise in H3 variants that differ based on age and tumor location. They associate with *TP53* mutations, or with activated neuro-developmental growth factor receptor pathways through distinct hits in *ACVR1*, *FGFR1* or *PDGFRA* to achieve tumorigenesis. These alterations in growth factor receptors and in members of the PI3K pathway offer previously unforeseen therapeutic possibilities in a deadly cancer, while the observed level of genomic instability calls for caution in the choice of adjuvant therapy whenever possible. Importantly, we show that small needle pre-therapy biopsies can reliably identify the mutational landscape in HGA. This will allow for tailoring available therapies to results obtained following stereotactic biopsy in children affected by this fatal brain tumor, while effort continues to be made to target K27M mutations.

Online Methods

Patient samples and consent

All samples were obtained with informed consent after approval of the Institutional Review Board of the respective hospitals they were treated in and were independently reviewed by senior pediatric neuropathologists (SA, KLL) according to the WHO guidelines. Samples were obtained from the Montreal Children's Hospital (Montreal, McGill University Health Centre), Boston Children's Hospital (Boston, Harvard University), Brain Tumor Toronto Bank (BTTB, Toronto, University Health Network) and collaborators in Hungary, in addition to previously midline high-grade astrocytoma published samples in[2,5] with sequencing data (n=11) and[4,5] with previously published DNA methylation data (n=89) for a total of 98 tumors included herein for DNA methylation and copy number variant (CNV) analysis. DIPG biopsy samples obtained pre-therapy were from DFCI protocol 10–321 (n=12), a prospective phase II biopsy study of newly diagnosed DIPG. The protocol is IRB approved through the Dana-Farber Harvard Cancer Center IRB, FDA IND #111,882, ClinicalTrials.gov Identifier NCT01182350, has local institutional approval at all participating sites and informed consent was obtained from all parents. Additional pediatric midline high-grade astrocytoma samples were from needle biopsies or partial resections prior to treatment (n=28). Sequencing and clinical data for this cohort is presented in Table S1, and methylation-derived CNVs in genes of interest are presented in Tables S4–5.

Whole-exome DNA sequencing

Standard genomic DNA extraction methods were performed according to described company protocols (Qiagen). Paired-end library preparations were carried out using the Nextera Rapid Capture Exome kit according to instructions from the manufacturer (Illumina) from 50 ng of total starting genomic DNA. Sequencing was performed in rapid run mode with 100 bp paired end reads on Illumina HiSeq 2000. We removed adaptor sequences and quality trimmed reads using the Fastx toolkit (http://hannonlab.cshl.edu/fastx_toolkit/) and then used a custom script to ensure that only read pairs with both mates present were subsequently used. Reads were aligned to hg19 with BWA 0.5.9[23], and indel realignment was done using the GATK[24]. Duplicate reads were then marked using Picard (http://picard.sourceforge.net/) and excluded from downstream analyses. We assessed coverage of consensus coding sequence (CCDS) bases using the GATK, which showed that

the majority of samples had >92% of CCDS bases covered by at least 10 reads, and >88% of CCDS bases covered by at least 20 reads.

For each sample, single nucleotide variants (SNVs) and short insertions and deletions (indels) were called using samtools mpileup[25] with the extended base alignment quality (BAQ) adjustment (-E), and were then quality filtered to require at least 20% of reads supporting the variant call. Variants were annotated using both Annovar[26] and custom scripts to identify whether they affected protein coding sequence, and whether they had previously been seen in the 1000 genomes dataset (Nov. 2011), the NHLBI GO exomes, or in approximately ~1000 exomes previously sequenced at our center. Useful links:

FASTX-Toolkit: http://hannonlab.cshl.edu/fastx_toolkit/

GATK: http://www.broadinstitute.org/gsa/wiki/

Picard tools: http://picard.sourceforge.net/

Samtools: http://samtools.sourceforge.net/

Variants in candidate genes of interest described herein in the midline HGA cohort (n=39) are detailed in Table S6.

MiSeq targeted high-depth DNA sequencing of *H3F3A*, *HIST1H3B* and *HIST1H3C*

Genomic DNA from midline HGA samples was utilized for high-depth sequencing of *H3F3A*, *HIST1H3B* and *HIST1H3C* genes to investigate the frequency of K27M reads in samples, notably those wild-type by whole-exome sequencing and high-resolution melting assays. Midline HGAs (n=24) were sequenced using the MiSeq sequencing platform (Illumina) and generated an average coverage of > 20,000X of the analogous K27M base change across the three histone variants (more specifically, for *H3F3A* gene, the average coverage is > 12,000X, for *HIST1H3B* it is > 12,000X, and for *HIST1H3C* the coverage is >35,000X). The reads were mapped to the reference genome (Human hg19) using bwa genome aligner[23]. The alignment files were fed to mpileup tool from SamTools package[25] in order to find all the variations without any filter applied by the conventional variant callers. An in-house parser program was developed to extract different variations at the desired positions (in this case, K27) in the mapped paired reads covering the histone genes *H3F3A*, *HIST1H3B* and *HIST1H3C*. The results are provided in Table S3.

RNA sequencing

RNA was extracted from patient tumor mHGA37 using the Qiagen RNeasy lipid tissue Mini Kit (Qiagen) according to instructions from the manufacturer. Library preparation was performed with ribosomal RNA (rRNA) depletion methods according to instruction from the manufacturer (Epicentre) to achieve greater coverage of mRNA and other long non-coding transcripts. Paired-end sequencing was performed on the Illumina HiSeq 2000 platform.

RNA-seq fusion analysis

RNA-seq Fastq files were utilized for fusion analysis using the deFuse software algorithm [27] according to indicated settings. Alorithmic output was then analyzed for high-confidence fusion transcripts, which were then re-constructed *in silico* utilizing online bioinformatics

tools and databases including Basic Local Alignment Search Tool, BLAST (http://blast.ncbi.nlm.nih.gov/Blast), Ensembl (http://useast.ensembl.org/index.html), UniProt (http://www.uniprot.org/) and the UCSC Genome Browser (http://genome.ucsc.edu) to assess impact on putative fusion proteins and compare them with existing, previously described fusions[8,17].

TERT promoter mutation sequencing

Characterized mutations in the *TERT* promoter, C228T, and C250T variants with G>A nucleotide substitutions at genomic positions 1,295,228 and 1,295,250 (hg19) respectively[28] were sequenced using the Sanger method in midline samples (n=14) and cortical samples (n=10) using the following cycling conditions: 96°C for 1min, 96°C for 10s, 60°C for 5s, 72°C for 1s, 72°C for 30s repeated for 33 cycles. Primer sequences are detailed in Table S8.

DNA methylation analysis

Extracted tumor DNA was analyzed for genome-wide DNA methylation patterns utilizing the HumanMethylation450 BeadChip platform according to instructions from the manufacturer (Illumina) and analyzed as described in[4,5]. From the selection of probes on the array, we removed probes from sex chromosomes (chrX and Y) as well as those located at sites with documented SNPs (as per dbSNP: http://www.ncbi.nlm.nih.gov/SNP/). Methylation values were normalized utilizing the Subset-quantile Within Array Normalization (SWAN) procedure provided in the R package minfi[29]. We performed hierarchical clustering using the 10,000 most variable sites. Distance was assessed using $d = 1 - r$, where r is the Pearson product-moment coefficient. Clustering was done using average linkage (UPGMA) and was validated for robustness of the procedure via multiscale resampling (1,000 iterations) using the R package pvclust [30] (Figure S6).

Copy number variant (CNV) detection

In order to assay CNV in our samples, we used a methylation-based method and controls implemented in the R/Bioconductor packages CopyNumber450k and CopyNumber450kData, respectively. CNV analysis for copy number gains and losses in previously described genes of interest is presented in Tables S4 and S5 respectively. Gross genomic aberrations were assessed using UCSC genome banding and our in-house algorithm described above. Bands covered with >90% significantly amplified or deleted segments were counted as “abnormal” and summed for each sample. Samples were grouped together by mutation type and a t-test was performed to assess statistically significant differences in aberration count between mutation subgroups. CNV analysis for broad areas of genomic instability is included in Table S7.

Cell lines and Western blotting

hTert-immortalized normal human astrocytes (NHA) were obtained from Dr Abhijit Guha (Labatt Brain Tumour Centre, Toronto, Canada) and were grown in DMEM supplemented with 10% FBS as previously described. DIPGIV primary cell line (kind gift of Dr. Michelle Monje, Stanford University, USA) and KNS42 (purchased from the JCRB) were grown as previously described[31]. Cell lines were serum/growth factor starved for 1 hour prior to

protein extraction. Proteins were extracted in Tris-NaCl-EDTA lysis buffer as previously described [32] and blotting was performed for phosphoSMAD1/5/8 (Cell Signaling Technology, #9511 at 1:500 dilution in 5% bovine serum albumin (BSA) solution) on total lysates from NHA cells and from DIPGIV cells as previously described[12]. Beta-actin (13E5) (Cell Signaling Technology) was used as loading control.

Quantitative PCR for BMP target genes

Quantitative PCR (qPCR) was performed to assess for levels of activity downstream of the ACVR1/ALK2 receptor in total RNA extracted from DIPGIV (H3,1K27M-ACVR1 G328V mutant) and KNS42 (H3.3G34V ACVR1 wild-type) and NHA cells grown in DMEM supplemented with 10% FBS using *ID1*, *ID2*, *ID3* and *SNAI1* using primer sequences detailed in Table S8. Briefly, total RNA was extracted using the miRNeasy mini kit (Qiagen) according to manufacturer's instructions with purity and integrity assessed utilizing Nanodrop (Thermo-Fisher) and Experion (Biorad) methodologies. 100ng of RNA was used for reverse-transcription using the iScript RT Supermix (BioRad) following manufacturer's instructions. Real-time PCR was run on a Lightcycler 96 (Roche) with the SsoFast Evagreen SuperMix kit (BioRad). Cycling conditions were: 95°C for 30 sec followed by 40 cycles 95°C for 5sec/60 °C for 20 sec. Fold change values were calculated utilizing the $2^{-\Delta\Delta Ct}$ method with *ACTB* expression and NHA cells used as the calibrator.

Immunohistochemistry

Immunohistochemistry (IHC) was performed on formalin-fixed, paraffin-embedded (FFPE) slides from patients with (n=4) or without *ACVR1* mutation (n=3) and control normal brain (n=1) to assess activation/phosphorylation of Smad1/5/8 downstream of the ACVR1/ALK2 receptor (reviewed in [33]). IHC was carried out as previously described[34] utilizing anti-phospho-Smad1/5/8 (Cell Signaling Technology, #9511) and anti-Smad1 (Invitrogen #38-5400). IHC processing and imaging was performed blind of *ACVR1* mutation status with representative images presented in Figure 2.

Fluorescence in-situ hybridization for *PDGFRA* amplification

Fluorescence in-situ hybridization (FISH) was performed as previously described in[35,36]. Briefly, FISH was performed utilizing 4μm thick tissue sections from a subset of midline HGAs, with a BAC probe directed towards the *PDGFRA* genomic locus at chromosomal region 4q12 (RP11-231c18, green) and a probe directed against 4p11.2-4q11.1 (CEN4, red) as a control to visualize chromosome 4. Scoring is included in Table S1, and representative images in Figure S2.

Supplementary Material

Refer to Web version on PubMed Central for supplementary material.

Acknowledgments

The authors would like to express their sincere gratitude toward all staff at the McGill University and Genome Quebec Innovation Centre for excellent technical expertise, library preparation and sequencing. This work was performed within the context of the I-CHANGE consortium (International Childhood Astrocytoma iNntegrated

Genomics and Epigenomics consortium) and supported by funding from Genome Canada, Genome Quebec, The Institute for Cancer Research of the Canadian Institutes for Health Research (CIHR) McGill University and the Montreal Children's Hospital Foundation. It was also supported by the Hungarian Scientific Research Fund (OTKA) Contract No. T-04639, the National Research and Development Fund (NKFP) Contract No. 1A/002/2004 (PH, MG) and TÁMOP-4.2.2A-11/1/KONV-2012-0025 (AK, LB). N. Jabado is a member of the Penny Cole lab and the recipient of a Chercheur Clinicien Senior Award. J. Majewski holds a Canada Research Chair (tier 2). We acknowledge the support of the Zach Carson DIPG Fund at the Dana-Farber Cancer Institute (DFCI), the Ellie Kavalieros Fund at DFCI, the Mikey Czech Foundation, the Prayer From Maria Foundation, the Hope for Caroline Fund at DFCI, the Ryan Harvey DIPG Fund at DFCI, the Stop&Shop Pediatric Brain Tumor Program at DFCI and the Pediatric Brain Tumor Clinical and Research Fund at DFCI. A.M.F. is supported by a studentship from the CIHR, as well as an award from the CIHR Systems Biology Training Program at McGill University. D. Bechet is supported by a studentship from the T.D trust/Montreal Children's Hospital Foundation and N. Gerges by a studentship from Cedars. N.D.J. is supported by an award from the McGill Integrated Cancer Research Training Program.

References

1. Khuong-Quang DA, et al. K27M mutation in histone H3.3 defines clinically and biologically distinct subgroups of pediatric diffuse intrinsic pontine gliomas. Acta Neuropathol. 2012; 124:439–47. [PubMed: 22661320]
2. Schwartzentruber J, et al. Driver mutations in histone H3.3 and chromatin remodelling genes in paediatric glioblastoma. Nature. 2012; 482:226–31. [PubMed: 22286061]
3. Wu G, et al. Somatic histone H3 alterations in pediatric diffuse intrinsic pontine gliomas and non-brainstem glioblastomas. Nat Genet. 2012
4. Sturm D, et al. Hotspot mutations in H3F3A and IDH1 define distinct epigenetic and biological subgroups of glioblastoma. Cancer Cell. 2012; 22:425–37. [PubMed: 23079654]
5. Fontebasso AM, et al. Mutations in SETD2 and genes affecting histone H3K36 methylation target hemispheric high-grade gliomas. Acta Neuropathol. 2013; 125:659–69. [PubMed: 23417712]
6. Paugh BS, et al. Genome-wide analyses identify recurrent amplifications of receptor tyrosine kinases and cell-cycle regulatory genes in diffuse intrinsic pontine glioma. J Clin Oncol. 2011; 29:3999–4006. [PubMed: 21931021]
7. Zarghooni M, et al. Whole-genome profiling of pediatric diffuse intrinsic pontine gliomas highlights platelet-derived growth factor receptor alpha and poly (ADP-ribose) polymerase as potential therapeutic targets. J Clin Oncol. 2010; 28:1337–44. [PubMed: 20142589]
8. Jones DT, et al. Recurrent somatic alterations of FGFR1 and NTRK2 in pilocytic astrocytoma. Nat Genet. 2013; 45:927–32. [PubMed: 23817572]
9. Shore EM, et al. A recurrent mutation in the BMP type I receptor ACVR1 causes inherited and sporadic fibrodysplasia ossificans progressiva. Nat Genet. 2006; 38:525–7. [PubMed: 16642017]
10. Fukuda T, et al. Generation of a mouse with conditionally activated signaling through the BMP receptor, ALK2. Genesis. 2006; 44:159–67. [PubMed: 16604518]
11. Chaikuad A, et al. Structure of the bone morphogenetic protein receptor ALK2 and implications for fibrodysplasia ossificans progressiva. J Biol Chem. 2012; 287:36990–8. [PubMed: 22977237]
12. Fukuda T, et al. A unique mutation of ALK2, G356D, found in a patient with fibrodysplasia ossificans progressiva is a moderately activated BMP type I receptor. Biochem Biophys Res Commun. 2008; 377:905–9. [PubMed: 18952055]
13. Mishina Y, Crombie R, Bradley A, Behringer RR. Multiple roles for activin-like kinase-2 signaling during mouse embryogenesis. Dev Biol. 1999; 213:314–26. [PubMed: 10479450]
14. Kishigami S, et al. BMP signaling through ACVRI is required for left-right patterning in the early mouse embryo. Dev Biol. 2004; 276:185–93. [PubMed: 15531373]
15. Miyazono K, Maeda S, Imamura T. BMP receptor signaling: transcriptional targets, regulation of signals, and signaling cross-talk. Cytokine Growth Factor Rev. 2005; 16:251–63. [PubMed: 15871923]
16. Korchynskyi O, ten Dijke P. Identification and functional characterization of distinct critically important bone morphogenetic protein-specific response elements in the Id1 promoter. J Biol Chem. 2002; 277:4883–91. [PubMed: 11729207]

17. Singh D, et al. Transforming fusions of FGFR and TACC genes in human glioblastoma. Science. 2012; 337:1231–5. [PubMed: 22837387]
18. Zhang J, et al. Whole-genome sequencing identifies genetic alterations in pediatric low-grade gliomas. Nat Genet. 2013; 45:602–12. [PubMed: 23583981]
19. Paugh BS, et al. Integrated molecular genetic profiling of pediatric high-grade gliomas reveals key differences with the adult disease. J Clin Oncol. 2010; 28:3061–8. [PubMed: 20479398]
20. Lewis PW, et al. Inhibition of PRC2 activity by a gain-of-function H3 mutation found in pediatric glioblastoma. Science. 2013; 340:857–61. [PubMed: 23539183]
21. Shen Q, et al. The fibrodysplasia ossificans progressiva R206H ACVR1 mutation activates BMP-independent chondrogenesis and zebrafish embryo ventralization. J Clin Invest. 2009; 119:3462–72. [PubMed: 19855136]
22. Lahti L, Peltopuro P, Piepponen TP, Partanen J. Cell-autonomous FGF signaling regulates anteroposterior patterning and neuronal differentiation in the mesodiencephalic dopaminergic progenitor domain. Development. 2012; 139:894–905. [PubMed: 22278924]
23. Li H, Durbin R. Fast and accurate short read alignment with Burrows-Wheeler transform. Bioinformatics. 2009; 25:1754–60. [PubMed: 19451168]
24. McKenna A, et al. The Genome Analysis Toolkit: a MapReduce framework for analyzing next-generation DNA sequencing data. Genome Res. 2010; 20:1297–303. [PubMed: 20644199]
25. Li H, et al. The Sequence Alignment/Map format and SAMtools. Bioinformatics. 2009; 25:2078–9. [PubMed: 19505943]
26. Wang K, Li M, Hakonarson H. ANNOVAR: functional annotation of genetic variants from high-throughput sequencing data. Nucleic Acids Res. 2010; 38:e164. [PubMed: 20601685]
27. McPherson A, et al. deFuse: an algorithm for gene fusion discovery in tumor RNA-Seq data. PLoS Comput Biol. 2011; 7:e1001138. [PubMed: 21625565]
28. Horn S, et al. TERT promoter mutations in familial and sporadic melanoma. Science. 2013; 339:959–61. [PubMed: 23348503]
29. Maksimovic J, Gordon L, Oshlack A. SWAN: Subset-quantile within array normalization for illumina infinium HumanMethylation450 BeadChips. Genome Biol. 2012; 13:R44. [PubMed: 22703947]
30. Suzuki R, Shimodaira H. Pvclust: an R package for assessing the uncertainty in hierarchical clustering. Bioinformatics. 2006; 22:1540–2. [PubMed: 16595560]
31. Monje M, et al. Hedgehog-responsive candidate cell of origin for diffuse intrinsic pontine glioma. Proc Natl Acad Sci U S A. 2011; 108:4453–8. [PubMed: 21368213]
32. Siegel PM, Ryan ED, Cardiff RD, Muller WJ. Elevated expression of activated forms of Neu/ErbB-2 and ErbB-3 are involved in the induction of mammary tumors in transgenic mice: implications for human breast cancer. EMBO J. 1999; 18:2149–64. [PubMed: 10205169]
33. Schmierer B, Hill CS. TGFbeta-SMAD signal transduction: molecular specificity and functional flexibility. Nat Rev Mol Cell Biol. 2007; 8:970–82. [PubMed: 18000526]
34. Kleinman CL, et al. Fusion of TTYH1 with the C19MC microRNA cluster drives expression of a brain-specific DNMT3B isoform in the embryonal brain tumor ETMR. Nat Genet. 2014; 46:39–44. [PubMed: 24316981]
35. Ramkissoon LA, et al. Genomic analysis of diffuse pediatric low-grade gliomas identifies recurrent oncogenic truncating rearrangements in the transcription factor MYBL1. Proc Natl Acad Sci U S A. 2013; 110:8188–93. [PubMed: 23633565]
36. Firestein R, et al. CDK8 is a colorectal cancer oncogene that regulates beta-catenin activity. Nature. 2008; 455:547–51. [PubMed: 18794900]

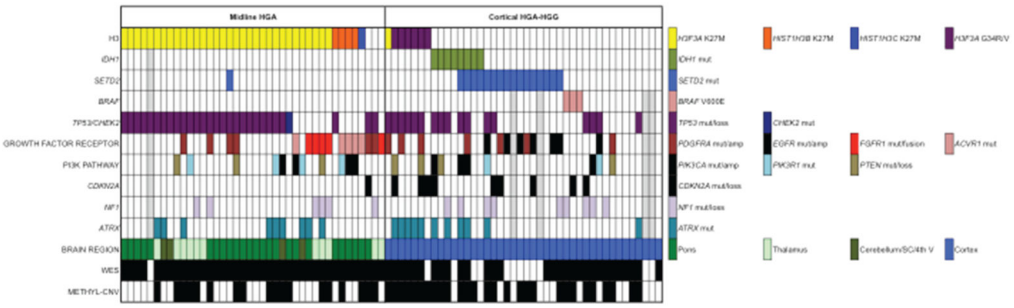

Figure 1. Genomic landscape of pediatric midline high-grade astrocytomas

Distribution of mutations and alterations in 40 pediatric midline high-grade astrocytomas (Midline HGAs) and 42 cortical high-grade astrocytomas and high-grade gliomas (Cortical HGA-HGGs) described in the study. Mutations (mut) were identified with whole-exome sequencing (WES) where available and are indicated by coloured boxes according to the legend in the right panel. Amplifications (amp) and losses were identified utilizing DNA methylation profile derived copy number variant (Methyl-CNV) analysis and are indicated where available by coloured boxes according to the right panel legend. SC = spinal cord, 4^{th} V = 4^{th} ventricle. Boxes coloured in light grey indicate samples for which data is not available. Detailed information regarding tumor samples included herein can be found in Table S1, with specific variants and transcript accessions presented in Table S6.

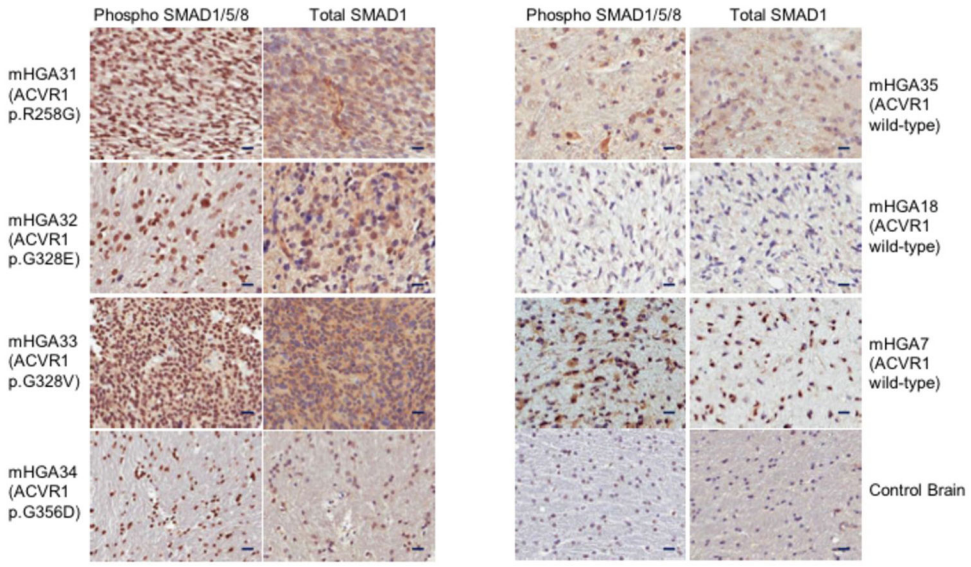

Figure 2. Increased levels of phospho-SMAD1/5/8 in ACVR1 mutant pediatric HGAs

Immunohistochemical analysis of midline pediatric HGAs harbouring *ACVR1* mutations identified in this study (n=4, left panels) demonstrate increased nuclear positivity of phospho-SMAD1/5/8 compared to pediatric midline HGAs wild-type for *ACVR1* mutation (n=3) and control brain samples (right panels), with total-SMAD1 staining shown in each case as positive control. Scale bars indicate 20X=20μm. Clinicopathologic and molecular characteristics of tumor samples are presented in Table S1.

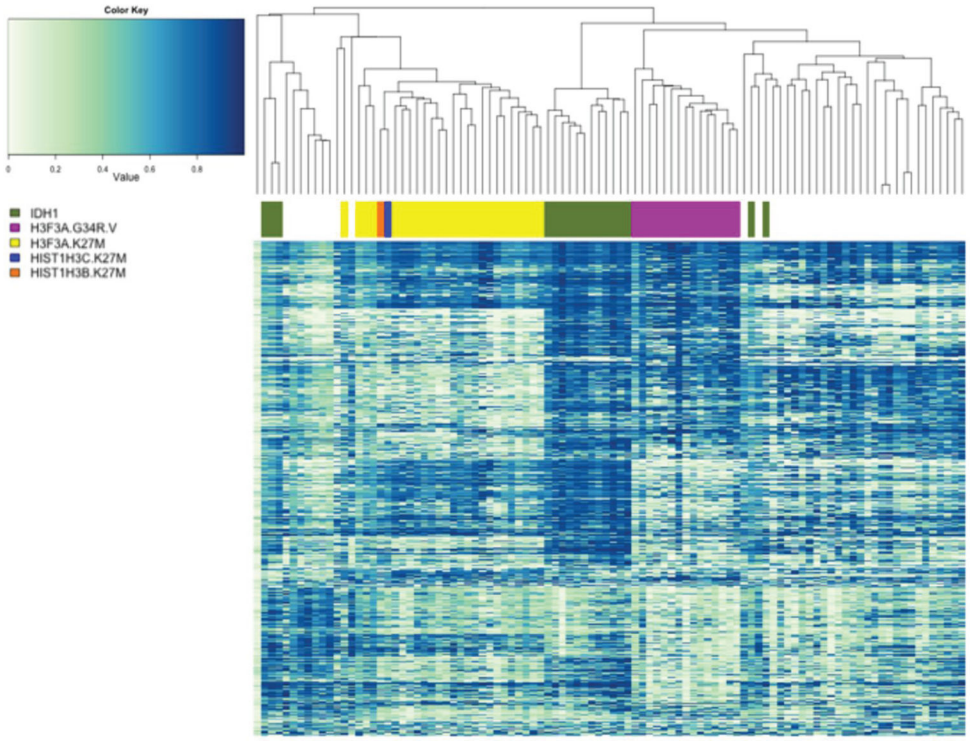

Figure 3. Clustering analysis of global DNA methylation profiles of 98 pediatric high-grade astrocytomas

Global DNA methylation clustering analysis of pediatric HGAs distributed across the brain demonstrates similar impact on epigenomic dysregulation caused by K27M mutation regardless of age, brain location, associated mutation or the particular histone 3 variant affected. The top 10,000 most variable normalized methylation β-values were utilized for UPGMA clustering with colour key and scale in top left panel, and indicated mutations of interest in inset left panel. Robustness was assessed utilizing multiscale bootstrapping in Figure S6. Detailed information regarding sample clinicopathologic characteristics are included in Table S1 with methylation-derived CNVs presented in Tables S4–5.

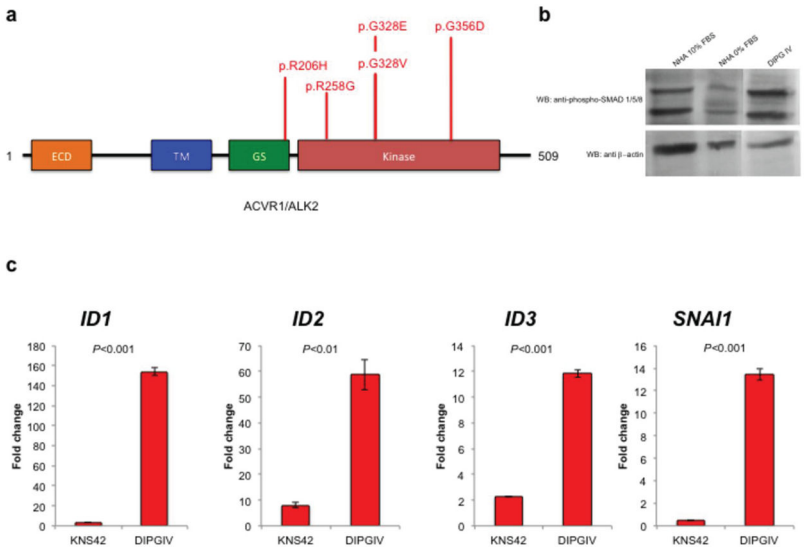

Figure 4. Mutations identified in *ACVR1* are associated with activation of downstream SMAD signaling pathways

a, Distribution of mutations identified in ACVR1 (n=5) demonstrating their impact of amino acid substitutions on the kinase domain of the protein. **b**, Immunoblotting analysis of phospho-SMAD1/5/8 levels in *ACVR1* wild-type NHA cells grown in 10% FBS, or NHA and DIPGIV (*ACVR1* G328V) serum starved for 1 hour in serum/growth factor-free media (0%). **c**, Quantitative PCR (qPCR) analysis of downstream BMP effectors *ID1*, *ID2*, *ID3* and *SNAI1* expression in ACVR1 mutant (DIPGIV) and wild-type GBM cell line (KNS42). Values represented are fold changes calculated using the $2^{-\Delta\Delta Ct}$ method, normalized to *ACTB* expression in calibrator NHA cells. *P*-values calculated using two-tailed T-test for significance, with error bars indicated as standard deviation from two replicates.